

Supporting Information: *Operando* scanning electron microscopy platform for *in situ* imaging of fluid evolution in nanoporous shale

*Artur Davletshin and Wen Song**

Center for Subsurface Energy and the Environment, The University of Texas at Austin,
Austin, Texas 78712, United States.

E-mail: wensong@utexas.edu

Microscale Imaging via ESEM-EDS

***In situ* SEM imaging.** *Operando* imaging of *in situ* fluid-mineral interactions was performed inside a high vacuum scanning electron microscope (FEI Quanta 650 ESEM, high vacuum $\sim 10^{-4}$ to 10^{-5} torr). The SEM was equipped with Everhart–Thornley detection (ETD) and energy dispersive X-ray spectroscopy (Bruker EDX). ETD was used for direct *in situ* visualization of organic matter thermolysis, fluid-mineral interactions, and matrix micro-fracturing under thermal stress. EDS spectroscopy was used for elemental mapping and mineral phase identification. Both ETD direct visualization and EDX elemental mapping of the pore morphology and connectivity of shale samples were achieved at a voltage of 30 kV. The spot size diameter used for imaging was ~ 6 to 7 nm.

Operando visualization was achieved for experiments conducted at the temperatures ranging from 20 °C to 450 °C.

Platform design. High temperature *in situ* imaging is enabled by inserting the visualization platform that isolates the fluid/solid sample from the SEM vacuum (Figure 1, main text) in an outer insulation case (Figure S1). Thermal insulation is achieved by a 15 mm thick layer of ceramic material (Alumina Ceramic, McMaster-Carr) that is held to the main visualization platform by an exterior stainless-steel case (Figure S1). The exterior cell thermally insulates the visualization platform from chamber detectors and the microscope stage. The maximum temperature of the outer stainless steel case was ~ 80 °C.

Operando temperatures of the shale sample was measured using a pair of K-type thermocouples that are attached to the compression cover of the visualization platform. Spatial variations in temperature measurements at the sample and the thermocouples (thermocouples are ~ 12 mm away from the material sample) are accounted for by calibrating the thermocouple data with direct temperature measurements taken on the sample (in vacuum, without visualization). Temperature measurements presented in the main text were adjusted using this calibration data (Figure S2).

Circuitry for the Arduino thermal control board is shown in Figure S3. A Tech HC-5 Bluetooth Serial Pass-through Module is connected to ports TX1 and RX0. Ports D4 through D10 are used to connect thermocouples. D10 is used for Relay connection.

Organic matter characterization. Organic matter composition of the shale samples was measured using pyrolysis (HAWK, Table S1). Samples were heated to temperatures of ~ 600 °C. Gas phase reaction products from thermochemical decomposition reactions were measured in the presence of an inert helium gas. Organic matter is categorized as S1 or S2.

S1 refers to the free hydrocarbons in the shale sample that are vaporized below temperatures of ~ 300 °C. S2 refers to the organic material that becomes converted to hydrocarbon fluids with thermal pyrolysis. We measure T_{\max} (i.e., temperature at which the maximum kerogen pyrolysis occurs) as an indicator for the maturity of the shale sample. Here, the T_{\max} occurs at a temperature of ~ 432 to 434 °C, indicating an immature/mature shale. Total organic carbon measures the sum of residual organic carbon and pyrolyzed organic carbon. Hydrogen and oxygen indices (HI, OI) were calculated to characterize the origin of the organic material; the high HI and low OI indicate marine origin for the shale samples used in this study.

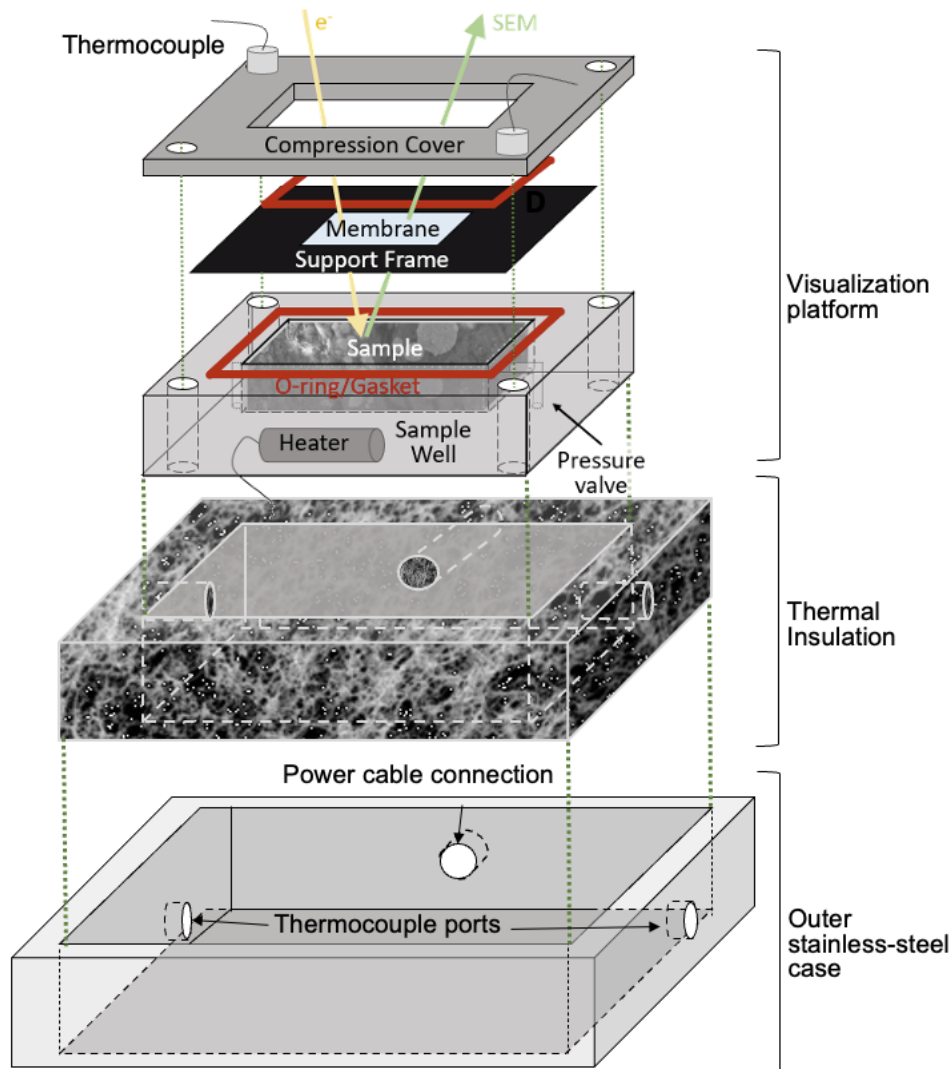


Figure S1. Thermally-compatible platform assembly for *operando* visualization during heating. The visualization platform discussed in the main text is insulated thermally from the SEM chamber using ceramic thermal insulation that is held within an outer stainless-steel case. Ceramic material (Alumina Ceramic, McMaster-Carr) is placed between the visualization platform and the outer stainless steel case. The outer stainless-steel case (316SS) encloses the insulation, with ports for thermocouple and heater power cable connections to the Arduino control board.

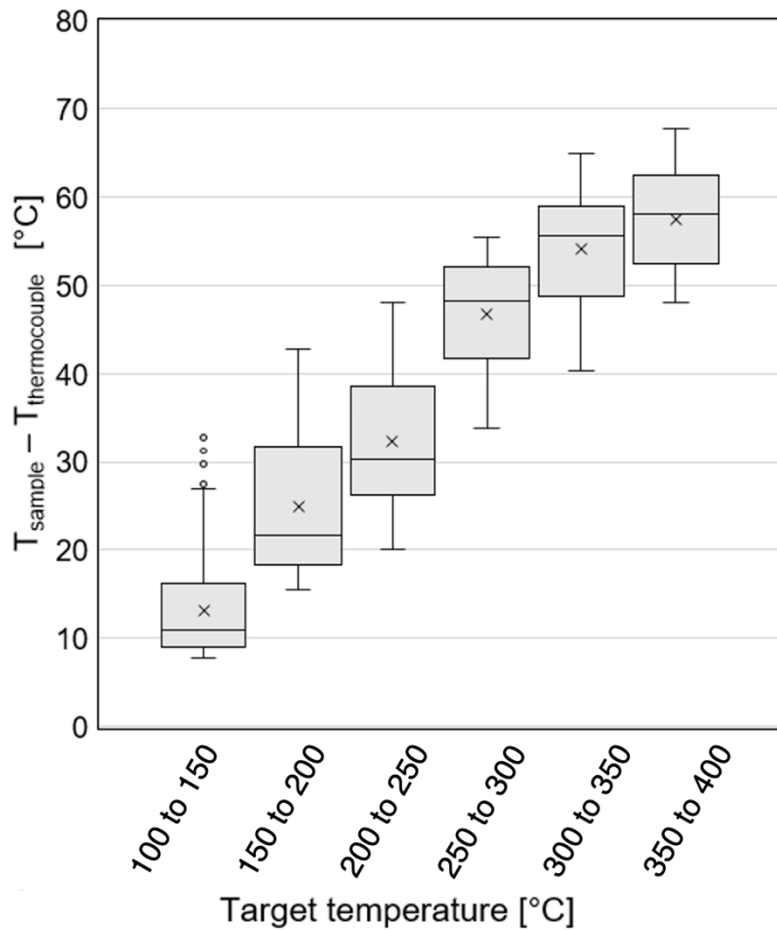


Figure S2. Calibration data for thermocouple measurements inside the sample well and on the compression cover measured in SEM vacuum.

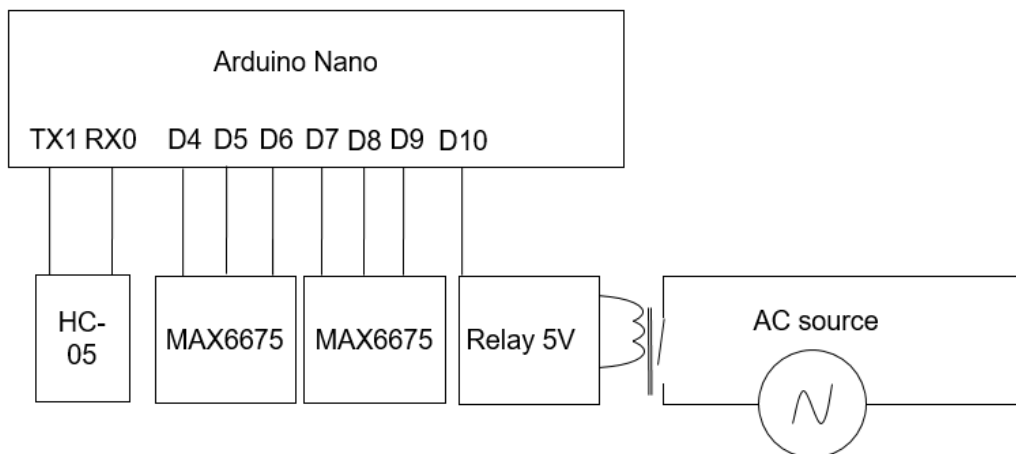


Figure S3. Arduino Control board circuit for enabling heat delivery and temperature measurements.

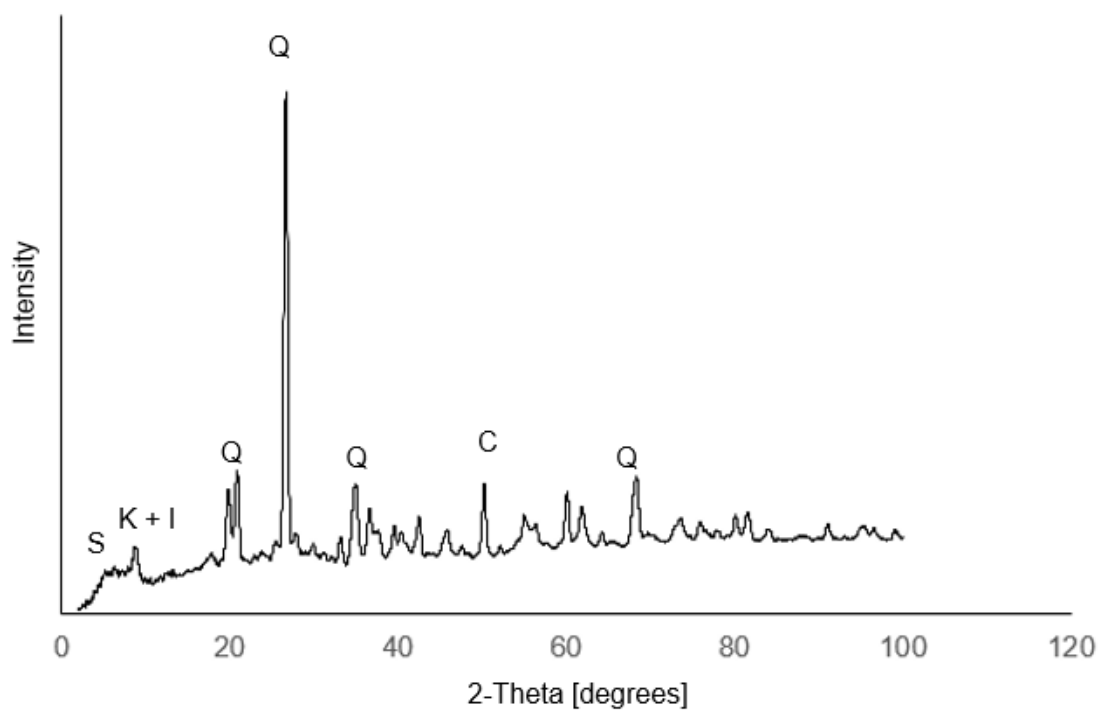


Figure S4. X-ray diffraction pattern of the shale sample. Major phases include quartz fragments (Q) and clay minerals kaolinite (K), illite (I), and smectite (S).

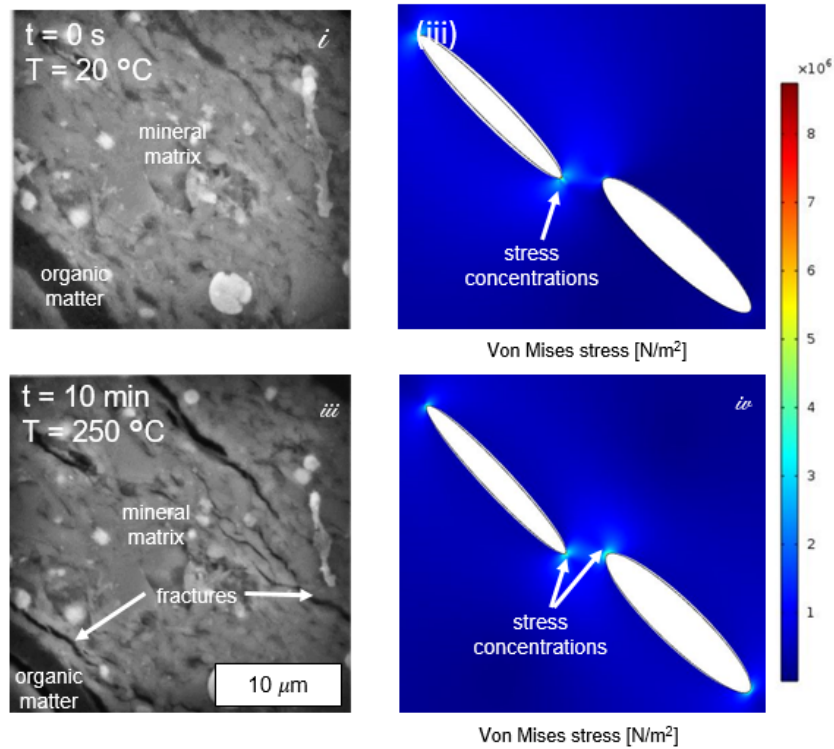


Figure S5. Microfracture generation in the shale mineral matrix by local thermo-chemical-mechanical stress. *Top-left and bottom left:* initial and stressed states of the shale sample, showing the nucleation and growth of microfractures initiating from the curved ends of organic matter undergoing thermolysis. *Top right and bottom right:* Numerical model of stress concentration showing localization around the curved kerogen tip. Here, low permeability through the mineral matrix results in a local pressure buildup. Stress concentration at the curved tips of the organic matter fragments suggest that fractures propagate preferably from the tips of the organic matter, which is consistent with experimental observations.

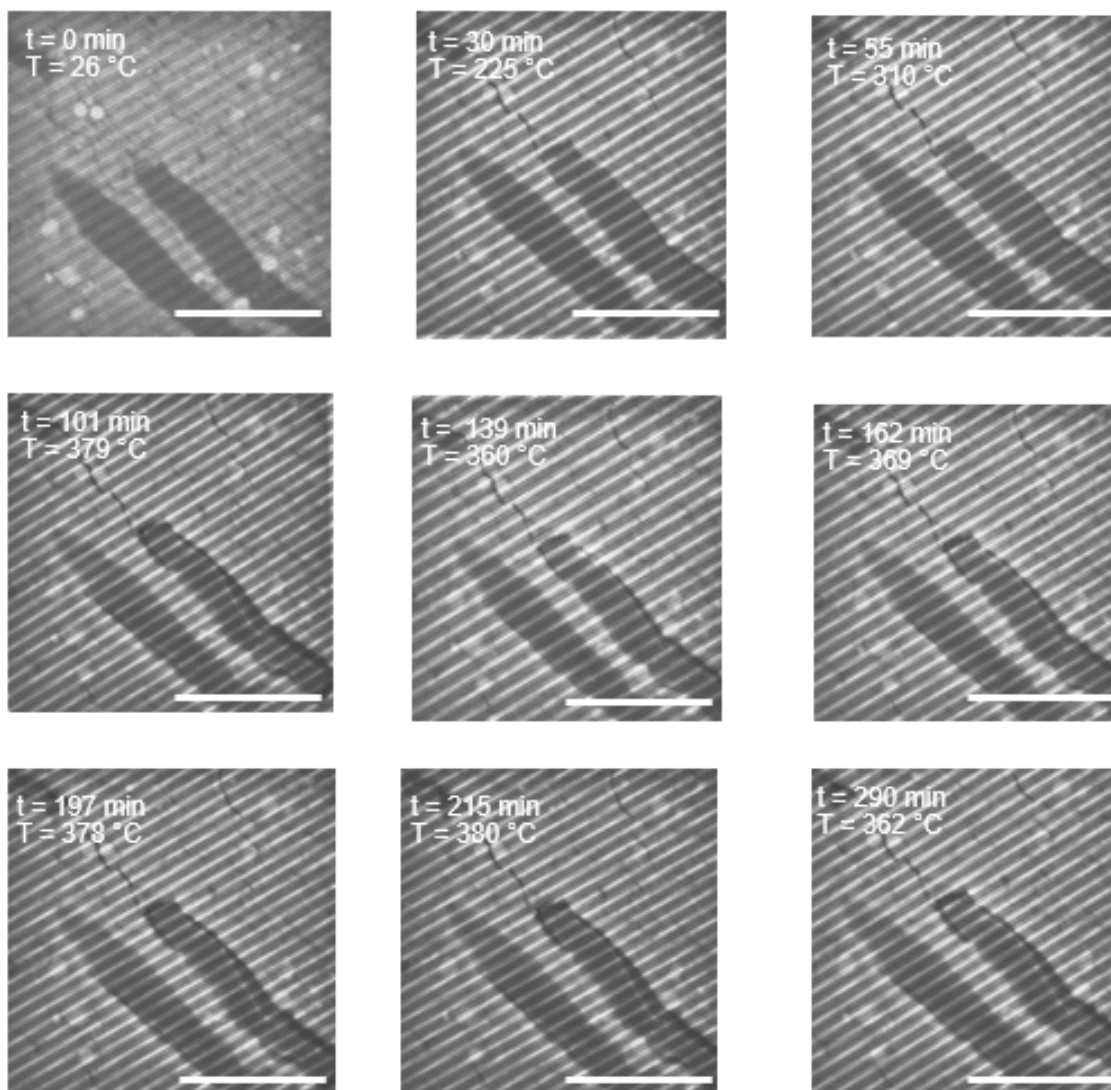


Figure S6. *Operando* SEM image series of organic matter fragments OM1 and OM2 in Figures 3B, C, and E during heating at elevated temperatures. Scale bar corresponds to the 50 μm . Parallel strips sloping from the top right to the bottom left are imaging artefacts of the SEM.

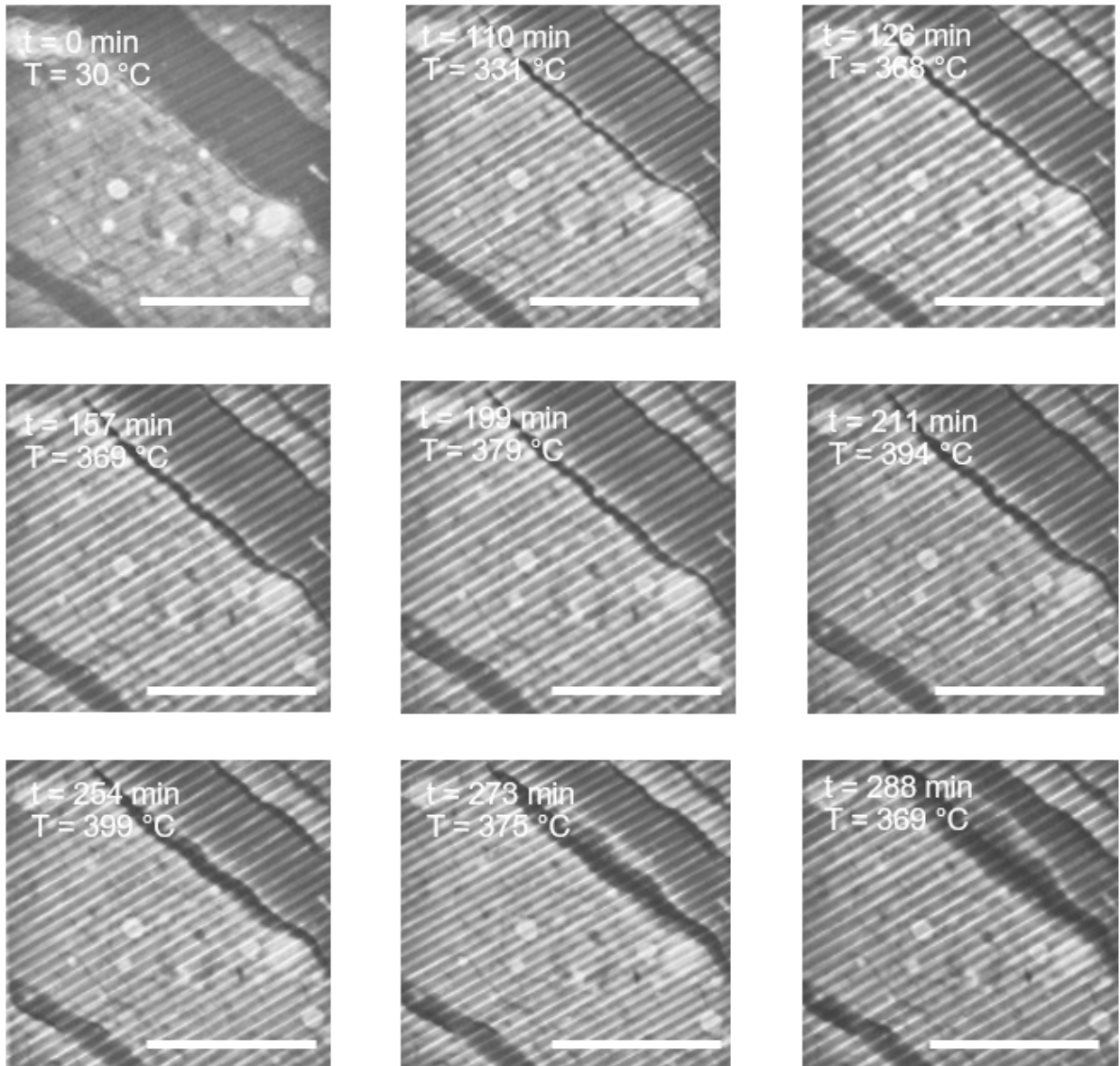


Figure S7. *Operando* SEM image series of the organic matter fragment used to compile Figure 3E (OM3) during heating at elevated temperatures. Scale bar corresponds to the 50 μm . Parallel strips sloping from the top right to the bottom left are imaging artefacts of the SEM.

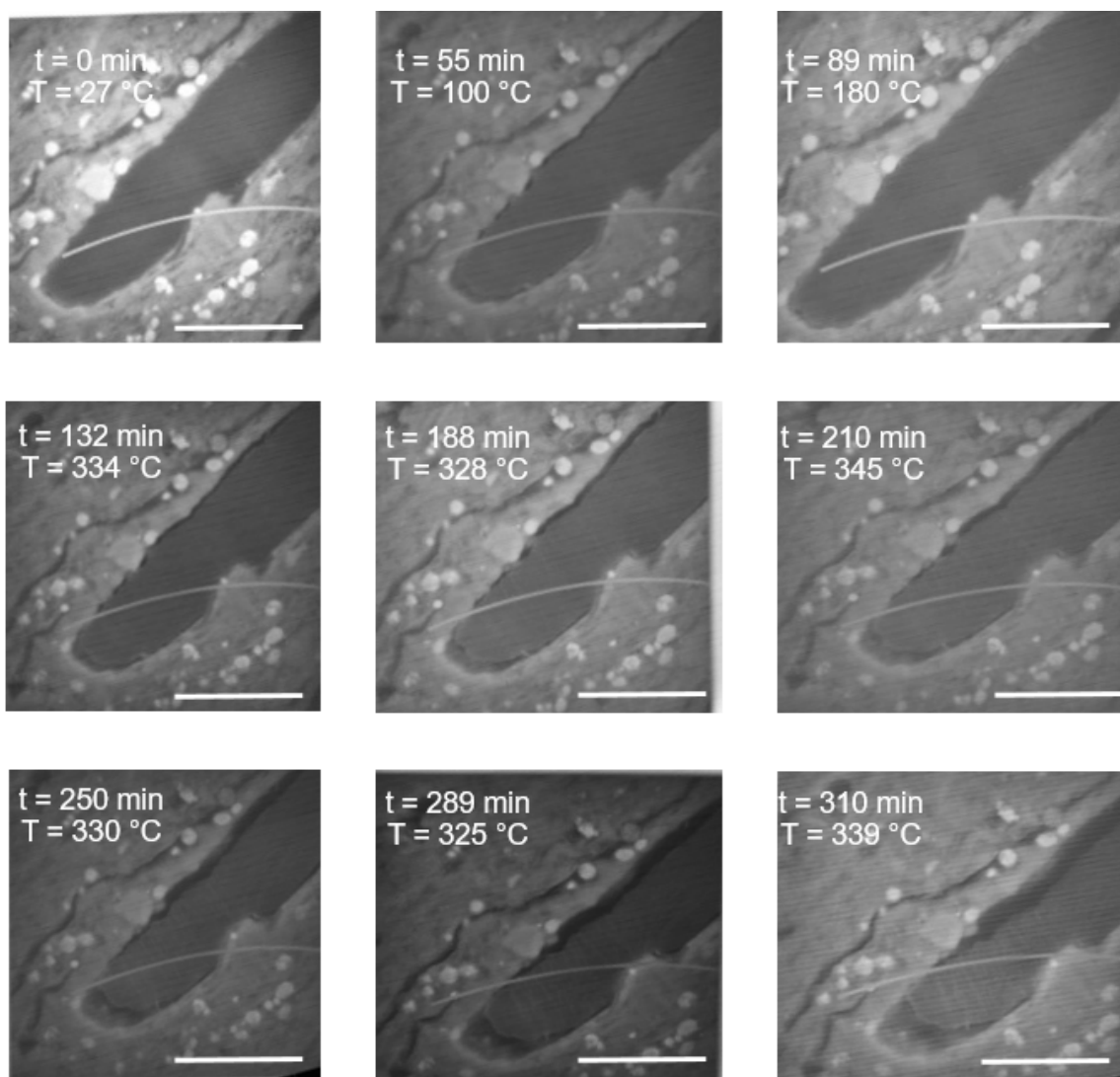


Figure S8. *Operando* SEM image series of the organic matter fragment used to compile Figure 3D during heating at elevated temperatures. Scale bar corresponds to the 50 μm.

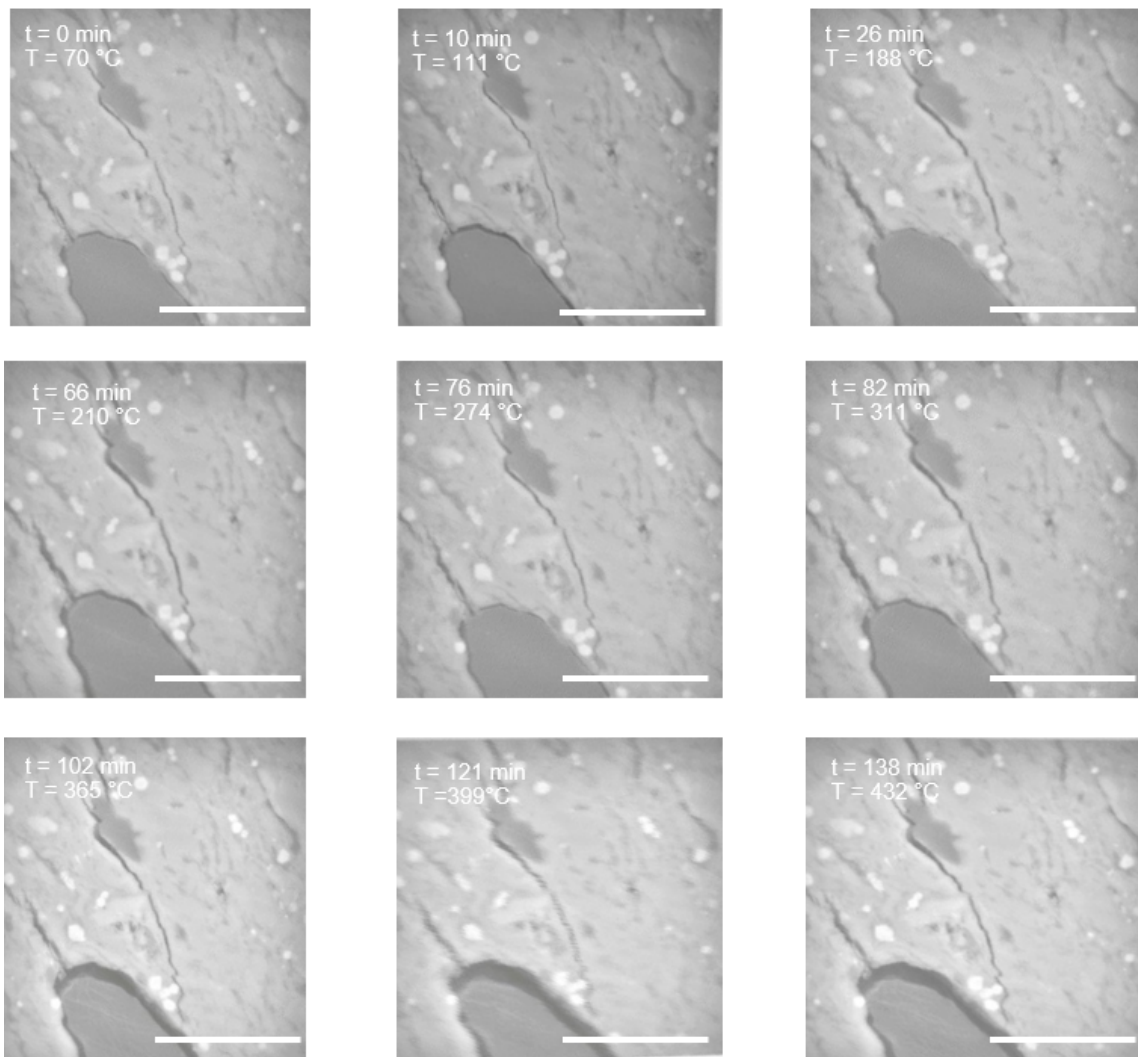


Figure S9. *Operando* SEM image series of microfracturing during heating at rates of ~ 3 °C/min used in Figure 2B. Scale bar corresponds to the 50 μm .

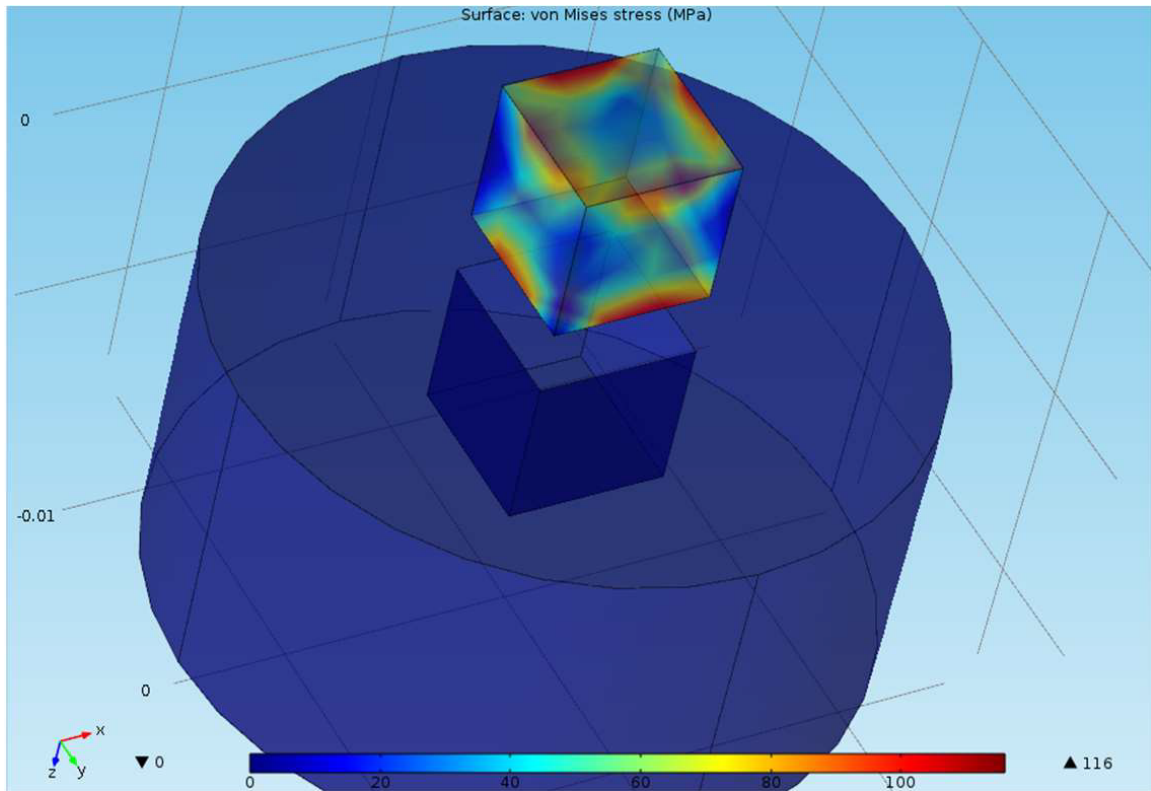


Figure S10. Finite element simulations of the internal stress of shale samples confined in the stainless steel sample well as a result of differential thermal expansion during heating experiments. Thermal expansion coefficients used were $17.2 \times 10^{-6} \text{ }^\circ\text{C}^{-1}$ for stainless steel and $20 \times 10^{-6} \text{ }^\circ\text{C}^{-1}$ for shale.

Table S1. HAWK-Eye Analysis Report.

Pyrolysis data	Range
Free Oil, S1 (mg _{HC} /g _{rock})	2.64 to 2.68
Kerogen yield, S2 (mg _{HC} /g _{rock})	55.84 to 56.9
Kerogen maturity, T _{max} (°C)	432 to 434
CO ₂ yield during kerogen pyrolysis, S3 (mg _{CO2} /g _{rock})	0.22 to 0.24
Total Organic Carbon, TOC (wt.%)	7.9 to 8.1
Hydrogen Index, HI (mg _{HC} /g _{TOC})	707 to 720
Oxygen Index, OI (mg _{CO2} /g _{TOC})	3 to 4

Table S2. Shale sample mineralogy measured using X-ray diffraction (XRD).

Phase	Mass fraction (wt.%)
Quartz	25.6
Clays (kaolinite, illite, smectite)	52.1
Remaining phases (calcite, rutile, muscovite, pyrite)	22.3

Table S3. R-squared and Mean Squared Error values for Figure 3D (main text).

	R²	Mean squared error
First Order Model	0.999	0.00145
Second Order Model	0.997	0.00147
N th Order Reaction, n = 3.9	0.992	0.00315

Movie S1 (separate file). *Operando* SEM movie of microfracture and pore development during heating to ~ 330 °C. Pores initiate and grow from the organic/mineral interface and, contrary to previous assertions, are not imaging artefacts.

Movie S2 (separate file). *Operando* SEM visualization of a moving liquid/vapor interface at ~ 390 °C. The fluids occupy pore space developed as a result of organic matter thermolysis during heating. Advancing and retreating contact angles are observed at mineral and organic surfaces.